

CAMI2V: CAMERA-CONTROLLED IMAGE-TO-VIDEO DIFFUSION MODEL

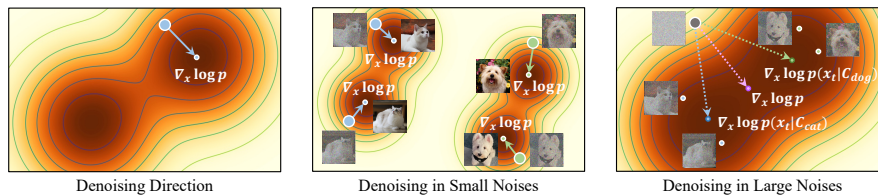
Guangcong Zheng, Teng Li, Rui Jiang, Yehao Lu, Tao Wu, Xi Li

College of Computer Science & Technology, Zhejiang University
 {guangcongzheng, xilizju}@zju.edu.cn

ABSTRACT

Recently, camera pose, as a user-friendly and physics-related condition, has been introduced into text-to-video diffusion model for camera control. However, existing methods simply inject camera conditions through a side input. These approaches neglect the inherent physical knowledge of camera pose, resulting in imprecise camera control, inconsistencies, and also poor interpretability. In this paper, we emphasize the necessity of integrating explicit physical constraints into model design. Epipolar attention is proposed for modeling all cross-frame relationships from a novel perspective of noised condition. This ensures that features are aggregated from corresponding epipolar lines in all noised frames, overcoming the limitations of current attention mechanisms in tracking displaced features across frames, especially when features move significantly with the camera and become obscured by noise. Additionally, we introduce register tokens to handle cases without intersections between frames, commonly caused by rapid camera movements, dynamic objects, or occlusions. To support image-to-video, we propose the multiple guidance scale to allow for precise control for image, text, and camera, respectively. Furthermore, we establish a more robust and reproducible evaluation pipeline to solve the inaccuracy and instability of existing camera control measurement. We achieve a 25.5% improvement in camera controllability on RealEstate10K while maintaining strong generalization to out-of-domain images. Only 24GB and 12GB are required for training and inference, respectively. We plan to release checkpoints, along with training and evaluation codes. Dynamic videos are best viewed at <https://zgctroy.github.io/CamI2V>.

(a) Explain the Principle of Condition:



(b) Extend the Definition of Condition:

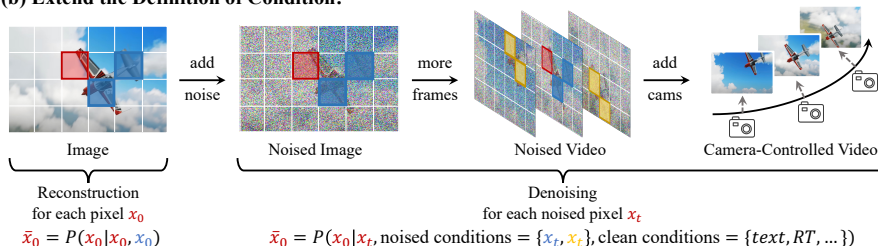


Figure 1: **Rethinking condition in diffusion models.** Diffusion models denoise along the gradient of log probability density function. At large noise levels, the high density region becomes the overlap of numerous noisy samples, resulting in visual blurriness. We point out that *the effectiveness of a condition depends on how much uncertainty it reduces*. From a new perspective, we categorize conditions into *clean conditions* (e.g. texts, camera extrinsics) that remain visible throughout the denoising process, and *noised conditions* (e.g. noised pixels in the current and other frames) whose deterministic information $\alpha_t x_0$ will be gradually dominated by the randomness of noise $\sigma_t \epsilon$.

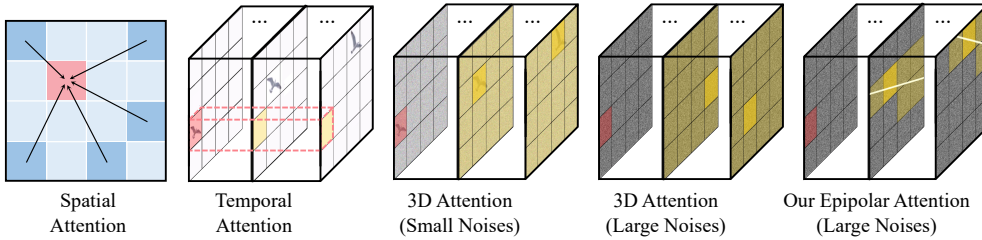


Figure 2: **Comparison of existing attention mechanisms for tracking displaced noised features.** Temporal attention is limited to features at the same location of picture, rendering it ineffective for significant camera movements. In contrast, 3D full attention facilitates cross-frame tracking due to its broad receptive field. However, high noise levels can obscure deterministic information, hindering consistent tracking. Our proposed epipolar attention aggregates features along the epipolar line, effectively modeling cross-frame relationships even under high noise conditions.

1 INTRODUCTION

The remarkable 3D consistency demonstrated in videos generated by Sora (Brooks et al., 2024) has highlighted the powerful capabilities of diffusion models (Ho et al., 2020; Rombach et al., 2022), showcasing their potential as a world simulator. Many researchers have attempted to enable the model to understand real-world knowledge (Chen et al., 2023a; Liu et al., 2023).

Condition or guidance (Ho & Salimans, 2022; Dhariwal & Nichol, 2021) is widely recognized as a crucial factor in enhancing generation quality. This is attributed to the fundamental principles that diffusion models denoise along the gradient of the log probability density function (score function) (Song et al., 2020), moving towards a high density region. However, this characteristic has varying effects at different noise levels (Tang et al., 2023a). As shown in Fig. 1(a), the high density region under high noise level becomes the overlap of numerous noisy samples, resulting in visual blurriness. By providing the model with conditions such as c_{dog} and c_{cat} , it can rapidly eliminate incorrect generations. This illustrates that effective conditions can guide the model towards desired outcomes while reducing uncertainty.

Consequently, incorporating physics-related or more detailed conditions into the diffusion model is an effective way of improving its world understanding. Considering that video generation requires providing condition for each frame, it is essential to identify a condition that is physics-related and also user-friendly. Recently, some camera-conditioned text-to-video diffusion models such as MotionCtrl (He et al., 2024a) and CameraCtrl (Wang et al., 2024d) have proposed using camera poses of each frame as a new type of condition. However, these methods simply inject camera conditions through a side input (like T2I-Adapter (Mou et al., 2024)) and neglect the inherent physical knowledge of camera pose, resulting in imprecise camera control, inconsistencies, and also poor interpretability. This raises a critical question: *How can we effectively inject camera poses into the diffusion model to enhance its ability to physical world knowledge?*

In this paper, we integrate geometric priors into the model and propose a novel framework for injecting camera poses. We first identify shortcomings in existing attention mechanisms regarding the ability of tracking noised features across frames. As illustrated in Fig. 2, separated spatial and temporal attention serves as an indirect form of 3D attention. The cross-frame interaction in temporal attention is confined to features at the same location in the image, rendering it ineffective for tracking significant movements resulting from large camera shifts. 3D full attention is widely applied in advanced video diffusion models such as OpenSora (Zheng et al., 2024) and CogVideoX (Yang et al., 2024b), due to its extensive receptive field. From the novel perspective of the noised conditions mentioned in Fig. 1, the broad receptive field of 3D full attention allows it to access more noised conditions. However, noised conditions act as a double-edged sword; at high noise levels, deterministic information is often obscured by random noise, resulting in minimal reduction of uncertainty despite increased access. As previously highlighted in Fig. 1, the quality of a condition is determined solely by its ability to reduce the model’s uncertainty, rather than by the number of conditions it can access.

To address these issues, we propose to apply plücker coordinates (Plücker, 1828) as absolute 3d ray embedding for implicit learning of 3d space and propose a novel epipolar attention mechanism that introduces an explicit constraint. This ensures that even when feature tracking is compromised under high noise conditions, only features along the epipolar line are aggregated. By doing so, our

approach minimizes the search space and reduces potential errors, ultimately enhancing 3D consistency across frames and improving overall controllability. Our explicit epipolar attention can also be regarded as a form of clean condition, as it reliably filters out features that do not conform to 3D geometry across varying noise levels, significantly enhancing controllability and stability. Additionally, inspired by Timothée et al. (2024), we incorporate register tokens into epipolar attention to address scenarios where there are no intersections between frames, often caused by rapid camera movements, dynamic objects, or occlusions.

For inference, we propose a multiple classifier-free guidance scale to control images, text, and camera respectively. If needed, several forward passes can be combined into a single pass by absorbing the scales of image, text, and camera into the model input, similar to timestep conditioning according to (Meng et al., 2023). For evaluation, we identify inaccuracies and instability in the current measurements of camera controllability due to the intrinsic limitations of SfM-based methods such as COLMAP (Schonberger & Frahm, 2016), which rely on identifying keypoint pairs and is quite challenging on generated videos with low resolution, high frame stride, and 3D inconsistencies. Considering the importance of accurate evaluation in this field, we establish a more robust, precise, and reproducible evaluation pipeline by implementing several enhancements. More details are provided in Section 5.

We conduct experiments on the RealEstate10k dataset and evaluate video generation quality using FVD (Unterthiner et al., 2018), as well as camera controllability metrics including RotError, TranError (Wang et al., 2024d), and CamMC (He et al., 2024a). The results demonstrate that the proposed epipolar attention mechanism across all noised frames significantly enhances geometric consistency and improves camera controllability. To facilitate further research, we will release all models trained on open-source frameworks such as DynamiCrafter, along with high-resolution checkpoints and training/evaluation codes, as soon as possible. To summarize, our key contributions are as follows:

- We expand the camera-conditioned text-to-video diffusion model to support reference image at random frame and propose multiple guidance scale to allow for precise control for text, image, and camera, respectively.
- From a novel perspective of noised condition, we propose epipolar attention added with register token as a explicit constraint for modeling all cross-frame relationships. This addresses the issue of noised features tracking due to the movement of camera, leading to precise camera control and better 3d consistency. It also reduces the controllability instability due to randomness introduced by noise during generation.
- We point out and analyze the reasons for inaccurate measurement of camera controllability caused by the inherent limitations of SfM evaluator and re-establish a more robust, accurate and reproducible evaluation pipeline. Furthermore, we achieve the sota performance on RealEstate10K dataset and out-of-domain dataset.

2 RELATED WORK

Diffusion-based Video Generation. With the advancement of diffusion models (Rombach et al., 2022; Ramesh et al., 2022; Zheng et al., 2022), video generation technology has progressed significantly. Given the scarcity of high-quality video-text datasets (Blattmann et al., 2023a;b), many researchers have sought to adapt existing text-to-image (T2I) models for text-to-video (T2V) generation. Some efforts involve integrating temporal blocks into original T2I models, training these additions to facilitate the conversion to T2V models. Examples include AnimateDiff (Guo et al., 2023), Align your Latents (Blattmann et al., 2023b), PYoCo (Ge et al., 2023), and Emu video (Girdhar et al., 2023). Additionally, methods such as LVDM (He et al., 2022), VideoCrafter (Chen et al., 2023a; 2024b), ModelScope (Wang et al., 2023a), LAVIE (Wang et al., 2023c), and VideoFactory Wang et al. (2024a) have adopted a similar structure, using T2I models as initialization weights and fine-tuning both spatial and temporal blocks to achieve better visual effects. Building on this foundation, Sora (Brooks et al., 2024) and CogVideoX (Yang et al., 2024b) have significantly enhanced video generation capabilities by introducing Transformer-based diffusion backbones (Peebles & Xie, 2023; Ma et al., 2024a; Yu et al., 2024) and leveraging 3D-VAE technology, thereby opening up the possibility of world simulators. Furthermore, works such as Dynamicrafter (Xing et al., 2023), SVD (Blattmann et al., 2023a), Seine (Chen et al., 2023b), I2vgen-XL (Zhang et al.,

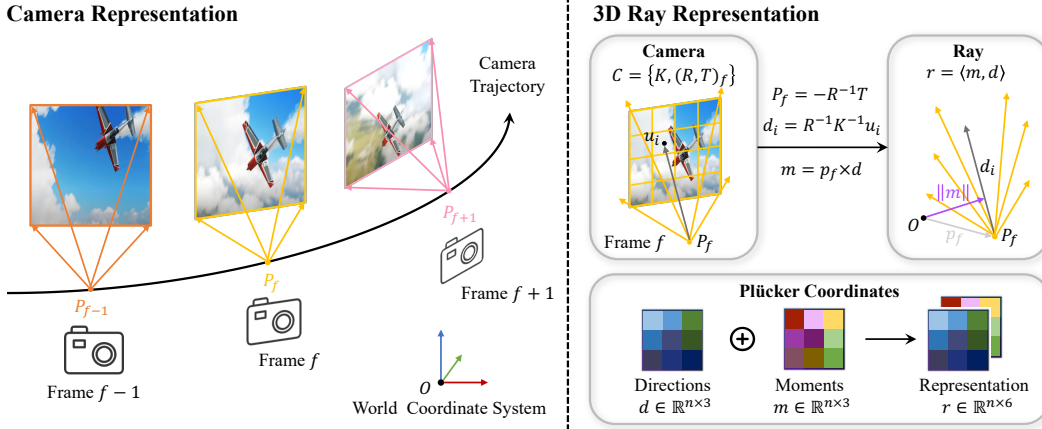


Figure 3: **Parameterizations for cameras.** Left: Camera representation and trajectory visualization in the world coordinate system. Right: The transformation from camera representations to 3D ray representations as Plücker coordinates given pixel coordinates.

2023b), and PIA (Zhang et al., 2024) have extensively explored image-to-video generation, achieving substantial progress.

Controllable Generation. With the development of image controllable generation technology (Zhang et al., 2023a; Jiang et al., 2024; Mou et al., 2024; Zheng et al., 2023; Peng et al., 2024; Ye et al., 2023; Wu et al., 2024b; Song et al., 2024; Wu et al., 2024d), video controllable generation has gradually become a highly focused direction. Significant progress has been made in areas such as pose (Ma et al., 2024b; Wang et al., 2023b; Hu, 2024; Xu et al., 2024b), trajectory (Yin et al., 2023; Chen et al., 2024a; Li et al., 2024; Wu et al., 2024a), subject (Chefer et al., 2024; Wang et al., 2024c; Wu et al., 2024c), and audio (Tang et al., 2023b; Tian et al., 2024; He et al., 2024b), greatly facilitating users to generate desired videos according to their needs.

Camera-controlled Video Generation. AnimateDiff (Guo et al., 2023) utilizes LoRA (Hu et al., 2021) fine-tuning to achieve specific camera movements. MotionMaster (Hu et al., 2024) and Peekaboo (Jain et al., 2024) explore a training-free method for coarse-grained camera movement generation, but they lack precise control. VideoComposer (Wang et al., 2024b) offers global motion guidance by adjusting pixel-level motion vectors. In contrast, MotionCtrl (Wang et al., 2024d), CameraCtrl (He et al., 2024a), and Direct-a-Video (Yang et al., 2024a) incorporate camera pose information as side input; however, these methods primarily focus on text-to-video generation and do not effectively leverage 3D geometric priors in camera pose. Concurrent work, CamCo (Xu et al., 2024a), also facilitates controllable camera generation in the image-to-video task by using epipolar lines to ensure consistency between generated frames and a single reference frame only. However, it does not account for scenarios where frames lack overlapping regions with the reference frame and can thus be regarded as a degenerate version of our approach.

3 METHOD

3.1 PRELIMINARIES

3D Ray Embedding. Considering camera intrinsics $K \in \mathbb{R}^{3 \times 3}$ and extrinsics (rotation $R \in \text{SO}(3)$, translation $T \in \mathbb{R}^3$), it parameterizes the transform from world coordinates to pixel coordinates by projection $u = K [R | T] x$. This low-dimensional representation may hinder neural networks from direct regression. Instead, we follow (Tseng et al., 2023) to represent cameras as ray bundles:

$$\mathcal{R} = \{r_1, \dots, r_n\}, \quad (1)$$

where each ray $r_i \in \mathbb{R}^6$ is associated with a known pixel coordinate u_i . Each ray r can be parameterized by ray direction $d \in \mathbb{R}^3$ from camera center $P \in \mathbb{R}^3$ as Plücker coordinates:

$$r = \langle m, d \rangle \in \mathbb{R}^6, \quad (2)$$

where $m = p \times d \in \mathbb{R}^3$ is the moment vector. When normalize d to unit length, the norm of the moment m represents the distance from the ray to the world origin. Given a set of 2D pixel

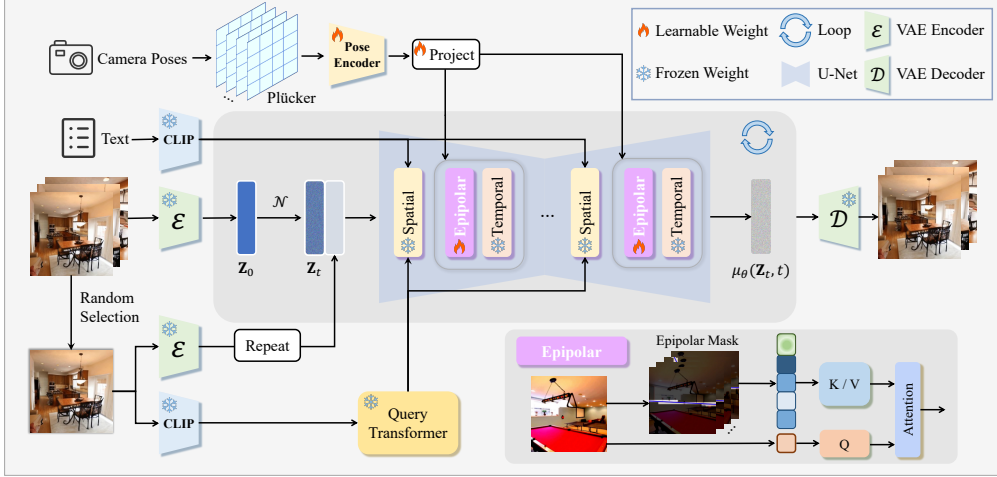


Figure 4: Pipeline of camera-conditioned image-to-video diffusion model.

coordinates $\{(u, v)_i\}^n$, ray directions d can be computed by the unprojection transform:

$$d = R^{-1}K^{-1} \cdot (u, v, 1)^T, m = (-R^{-1}T) \times d \quad (3)$$

Text-guided Image to Video Diffusion Model. Text-guided Image to Video Diffusion Model (Zhang et al., 2024; 2023b; Xing et al., 2023) learn a video data distribution by the gradual denoising of a variable sampled from a Gaussian distribution. For image to video generation, first, a learnable auto-encoder (consisting of an encoder \mathcal{E} and a decoder \mathcal{D}) is trained to compress the video into latent space. Then, a latent representation $z = \mathcal{E}(x)$ is trained instead of a video x . Specifically, the diffusion model ϵ_θ aims to predict the added noise ϵ at each timestep t based on the text condition c_{txt} and the reference image condition c_{img} , where $t \in \mathcal{U}(0, 1)$. The training objective can be simplified as a reconstruction loss:

$$\mathcal{L} = \mathbb{E}_{z, c_{\text{txt}}, c_{\text{img}}, \epsilon \sim \mathcal{N}(0, I), t} \left[\|\epsilon - \epsilon_\theta(z_t, c_{\text{txt}}, c_{\text{img}}, t)\|_2^2 \right], \quad (4)$$

where $z \in \mathbb{R}^{F \times H \times W \times C}$ is the latent code of video data with F, H, W, C being frame, height, width, and channel. Besides, c_{txt} is the text prompt for input video, and c_{img} is the reference frame of video. A noise-corrupted latent code z_t from the ground-truth z_0 is formulated as $z_t = \alpha_t z_0 + \sigma_t \epsilon$, where $\sigma_t = \sqrt{1 - \alpha_t^2}$, α_t and σ_t are hyperparameters to control the diffusion process.

3.2 OVERALL PIPELINE

In this section, we present our novel camera-conditioned method for geometry-consistent image-to-video generation, as shown in Fig. 4. We first describe cross-frame epipolar line and discretized epipolar mask, grounded in the principle of camera projection. Next, we propose epipolar-constrained attention module for the base model in a plug-and-play manner, which effectively make use of feature correlations along epipolar lines. Further, we discuss the situation when epipolar lines of all frames are outside the image plane and introduce register tokens as a simple yet effective fix. Finally, we leverage multiple CFG to balance visual quality and camera pose consistency.

3.3 EPIPOLAR ATTENTION FOR NOISED FEATURES TRACKING

Epipolar line and mask. The proposed epipolar attention mechanism seeks to establish a connection between frames, as shown on the left-hand side of Fig. 5. Its primary concept involves utilizing the epipolar line as a constraint, which effectively narrows down the potential matching pixels from one target frame to any other frames. For a single pixel at coordinate (u, v) on the i -th frame, the corresponding epipolar line $l_{ij} \in \mathbb{R}^3$ on the j -th frame can be formulated as:

$$l_{ij}(u, v) = F_{ij} \cdot (u, v, 1)^T, \quad (5)$$

where F_{ij} is the camera fundamental matrix of two frames, which can be derived as $F_{ij} = K_j^{-T} \cdot E_{ij} \cdot K_i^{-1}$ given the camera intrinsics $K_i, K_j \in \mathbb{R}^{3 \times 3}$ and the camera essential matrix $E_{ij} \in \mathbb{R}^{3 \times 3}$.

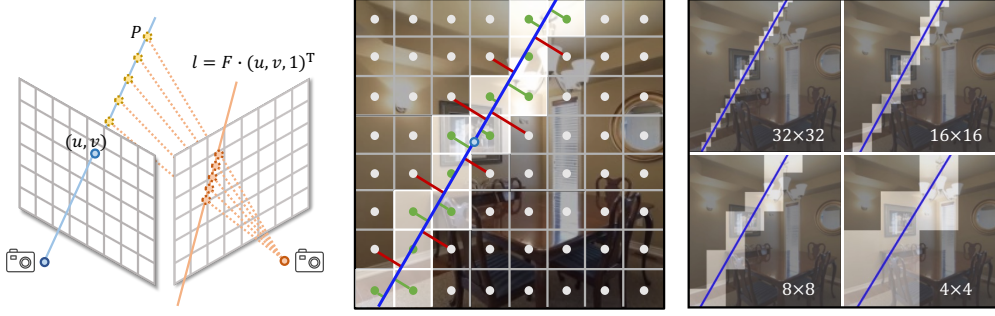


Figure 5: **Epipolar line and mask.** Left: Epipolar constraint of the j -th frame from one pixel at (u, v) on the i -th frame. Middle: Epipolar mask discretized by the distance threshold δ , so that only neighboring pixels in green are allowed to attend while those red lined are not. Right: Multi-resolution epipolar mask adaptive to the feature size in U-Net layers.

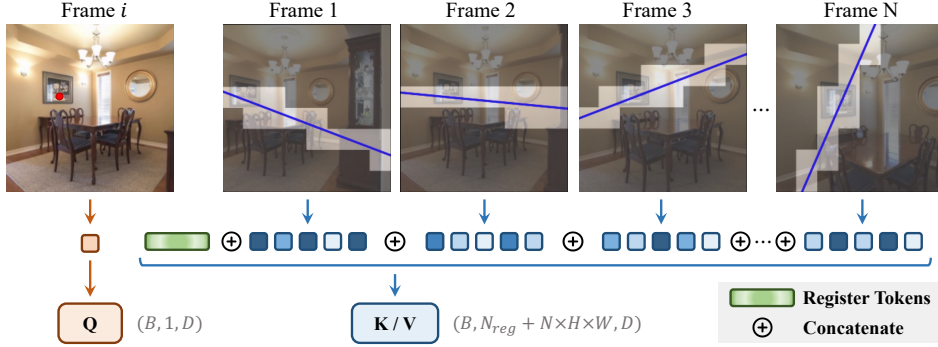


Figure 6: **Epipolar attention mask with register tokens.** We specify query pixel by red point in the i -th frame for clarity. Epipolar attention mask is constructed by concatenating epipolar masks along all frames. We insert register tokens to key/value sequence to deal with zero epipolar scenarios.

We transform the camera pose of the j -th frame to be relative to the i -th frame for simplicity, thus it holds that $E_{ij} = T_{i \rightarrow j} \times R_{i \rightarrow j}$, where $R_{i \rightarrow j} \in \mathbb{R}^{3 \times 3}$ and $T_{i \rightarrow j} \in \mathbb{R}^3$ are the relative rotation matrix and translation vector, respectively. Due to the contiguous representation of the epipolar line $l_{ij} = Ax + By + C$, we convert it to attention mask by calculating per-pixel distance at coordinate (u', v') on the j -th frame to the epipolar line as

$$d_{ij}(u', v') = \frac{(A, B, C) \cdot (u', v', 1)}{\sqrt{A^2 + B^2}}, \quad (6)$$

and filtering out those values that are larger than a threshold δ . We empirically choose half of the diagonal of the feature grid size as the threshold. This approach optimizes the correspondence search space by significantly reducing the number of candidates from hw to l , with $l \ll hw$, thereby enhancing efficiency and accuracy.

Epipolar attention. We extend current temporal attention with epipolar constraint to leverage cross-frame relationship and inject geometry consistency for video generation. We denote the noised latent of the i -th frame at timestamp t as $z_t^i \in \mathbb{R}^{hw \times c}$. And the query, key and value are defined as $q = W_q z_t^i \in \mathbb{R}^{hw \times c}$, $k = W_k \{z_t^j\}_{j=1}^N \in \mathbb{R}^{Nhw \times c}$ and $v = W_v \{z_t^j\}_{j=1}^N \in \mathbb{R}^{Nhw \times c}$, where W_q , W_k and W_v are the projection matrices respectively. Given the epipolar attention mask $m_i \in \mathbb{R}^{hw \times Nhw}$ introduced in Section 3.3, our epipolar attention that captures relevant contextual information between the i -th frame and all N frames is then computed as

$$\text{EpipolarAttn}(z_t^i, \{z_t^j\}_{j=1}^N, m_i) = \text{softmax} \left(\frac{qk^T}{\sqrt{d}} \odot m_i \right) v, \quad (7)$$

where \odot denotes Hadamard product and d is the dimension of attention heads for attention score normalization. For detailed computation procedures, please refer to Appendix A.

Register tokens for special cases. For videos with significant camera movements, dynamic objects, or occlusions, there may be cases where some pixels from the i -th frame have no corresponding epipolar lines within the image planes of all N frames. This situation can lead to a zero epipolar mask, affecting the computational stability of the epipolar attention mechanism.

To address this issue, we draw inspiration from Timothée et al. (2024) and introduce additional register tokens to the input sequence as a straightforward solution, as illustrated in Fig. 6. Additionally, register tokens are learnable, enabling adaptive learning to address various special cases.

3.4 MULTIPLE CLASSIFIER-FREE GUIDANCE

Control for multiple condition. Similar to DynamicCrafter (Xing et al., 2023; Esser et al., 2023), we introduce two guidance scales $s_{\text{img\&txt}}$ and s_{camera} to text-conditioned image animation, which can be adjusted to trade off the impact of two control signals:

$$\begin{aligned} \hat{\epsilon}_\theta(\mathbf{z}_t, \mathbf{c}_{\text{camera}}, \mathbf{c}_{\text{img\&txt}}) &= \epsilon_\theta(\mathbf{z}_t, \mathbf{c}_{\text{camera}}, \emptyset) \\ &+ s_{\text{img\&txt}}(\epsilon_\theta(\mathbf{z}_t, \mathbf{c}_{\text{camera}}, \mathbf{c}_{\text{img\&txt}}) - \epsilon_\theta(\mathbf{z}_t, \mathbf{c}_{\text{camera}}, \emptyset)) \\ &+ s_{\text{camera}}(\epsilon_\theta(\mathbf{z}_t, \mathbf{c}_{\text{camera}}, \mathbf{c}_{\text{img\&txt}}) - \epsilon_\theta(\mathbf{z}_t, \emptyset, \mathbf{c}_{\text{img\&txt}})). \end{aligned} \quad (8)$$

Multiple scale distillation for acceleration. If needed, we can distill (Xing et al., 2023) the two guidance scales $s_{\text{img\&txt}}$ and s_{camera} into the model to further avoid the extra inference time brought by three times of forward:

$$\epsilon_\theta(\mathbf{z}_t, \mathbf{c}_{\text{camera}}, \mathbf{c}_{\text{img\&txt}}, s_{\text{camera}}, s_{\text{img\&txt}}) = \hat{\epsilon}_\theta(\mathbf{z}_t, \mathbf{c}_{\text{camera}}, \mathbf{c}_{\text{img\&txt}}) \quad (9)$$

4 METRICS AND EVALUATION

In this section, we present our reproducible evaluation pipeline. Previous studies have employed various evaluation protocols, resulting in inconsistent metrics due to the lack of a common benchmark. The structure-from-motion (SfM) method such as COLMAP (Schonberger & Frahm, 2016), struggles to produce stable and accurate predictions when applied to generated videos. This challenge arises because SfM relies on SIFT operators for keypoint identification, which can lead to erroneous matches when assessing generated content. Such inaccuracies may result in unsolvable equations or significantly flawed estimates of camera extrinsics. Contributing factors include the low resolution of these videos (256x256), the presence of dynamic scenes, the absence of true 3D consistency, and issues related to lighting variations and object distortion.

To address these limitations, we adapt the global structure-from-motion method GLOMAP (Pan et al., 2024) to validate camera pose consistency. Our evaluation pipeline comprises three steps: feature extraction, exhaustive matching, and global mapping. To enhance robustness, we share GT priors for camera intrinsics (f_x, f_y, c_x, c_y) and allow the structure-from-motion process to focus primarily on optimizing camera extrinsics. Detailed CLI parameters can be found in Appendix B.

Before calculating metrics, we canonicalize the estimated camera-to-world matrices by converting each frame relative to the first frame and normalizing the scene scale using the \mathcal{L}_2 distance from the first camera to the furthest cameras. To account for randomness introduced by GLOMAP, we conduct five individual trials for each of the 1,000 sampled videos, averaging only those trials that are successful per sample. The final metrics, including RotErr, TransErr, and CamMC, are averaged on a sample-wise basis.

RotError. We evaluate per-frame camera-to-world rotation accuracy by the relative angles between ground truth rotations R_i and estimated rotations \tilde{R}_i of generated frames. We report accumulated rotation error along 16 frames in radians.

$$\text{RotErr} = \sum_{i=1}^n \cos^{-1} \frac{\text{tr}(\tilde{R}_i R_i^T) - 1}{2} \quad (10)$$

TransError. We evaluate per-frame camera trajectory accuracy by the camera location in the world coordinate system, i.e. the translation component of camera-to-world matrices. We report the sum

of \mathcal{L}_2 distance between ground truth translations T_i and generated translations \tilde{T}_i for all 16 frames.

$$\text{TransErr} = \sum_{i=1}^n \left\| \tilde{T}_i - T_i \right\|_2 \quad (11)$$

CamMC. We also evaluate camera pose accuracy by directly calculating \mathcal{L}_2 similarity of per-frame rotations and translations as a whole. We sum up the results of 16 frames.

$$\text{CamMC} = \sum_{i=1}^n \left\| [\tilde{R}_i | \tilde{T}_i] - [R_i | T_i] \right\|_2 \quad (12)$$

FVD. Additionally, to ensure that proposed method coherently improve generative capability and visual quality of base I2V model, we evaluate the distance of generated frames from training distribution by Fréchet Video Distance (FVD) (Unterthiner et al., 2018)¹.

5 EXPERIMENTS

5.1 SETUP

Dataset. We train our model on RealEstate10K (Zhou et al., 2018) dataset, which contains approximately 70K video clips at the resolution of around 720P with camera poses annotated by SLAM-based methods. We resize video clips from dataset to 256 while keeping the original aspect ratio and perform center cropping to fit in our training scheme. We sample 16 frames from single video clip when training with a random frame stride ranging from 1 to 10. We set fixed frame stride of 8 for inference. We take random condition frame for generation as data augmentation.

Implementation Details. We choose DynamiCrafter (Xing et al., 2023) as our base image-to-video (I2V) model and implement proposed method on the top of it. For fair comparison, we also make reproduction work of MotionCtrl (Wang et al., 2024d) and CameraCtrl (He et al., 2024a), since their public accessible versions are either T2V or SVD-based. We project Plücker embedding into base model by a pose encoder similar to the architecture in CameraCtrl. We freeze all parameters from base model and train proposed method at the resolution of 256×256 . We set 2 register tokens for the epipolar module to attend when no relevant pixels are on the epipolar line. We apply the Adam optimizer with a constant learning rate of 1×10^{-4} . We follow DynamiCrafter to choose Lightning as our training framework with mixed-precision fp16 and DeepSpeed ZeRO-1. We train proposed method and variants on 8 NVIDIA 3090 GPUs with effective batch size of 64 for 50K steps.

5.2 QUANTITATIVE COMPARISON

We compare our CAMI2V with the latest methods in camera controlled image-to-video generation, including DynamiCrafter (Xing et al., 2023), MotionCtrl (Wang et al., 2024d) and CameraCtrl (He et al., 2024a). As reported in Table 1, our CAMI2V significantly improves the camera controllability, with substantial reductions in RotErr, TransErr and CamMC. Compared to MotionCtrl, our method reduces RotErr by 0.512, translating to a 3.67° decrease in rotational error, which marks a significant improvement. However, enhancing camera controllability inevitably leads to a decline in FVD. Nevertheless, our method surpasses the state-of-the-art method CameraCtrl in both camera controllability and FVD metrics.

5.3 ABLATION STUDY

We conduct ablation study of proposed method on Plücker embedding, 3D full attention and our proposed epipolar attention. All model variants are trained under the same protocol mentioned in Section 5.1 for 50K steps. Evaluation results under CFG $s_{\text{img\&txt}} = 4$ and $s_{\text{camera}} = 1.875$ are provided in Table 2. In this section, we will discuss the validity of our Plücker pose encoder and epipolar-constrained attention module.

Plücker embedding. The experimental results illustrate that Plücker embedding significantly enhance the capability of base model for camera control. It also coherently improve visual quality of

¹We use “fvdcal” to calculate FVD metric.

Table 1: **Quantitative comparison with state-of-the-art methods.** Our method achieves a significant improvement in camera controllability (25.5% in rotation and 7.77% in translation compared to previous sota), where a decrease of 0.1 in RotErr corresponds to a reduction of 0.72 degrees in rotational error. * denotes the results we reproduced using DynamiCrafter as base I2V model.

Method	Publication	TransErr↓	RotErr↓	CamMC↓	FVD↓	
					VideoGPT	StyleGAN
DynamiCrafter	ECCV 2024	9.674	3.086	11.28	113.25	97.181
DynamiCrafter+MotionCtrl*	SIGGRAPH 2024	2.632	0.955	3.197	72.073	62.069
DynamiCrafter+CameraCtrl*	arXiv 2024	1.636	0.595	1.958	78.795	66.916
DynamiCrafter+CamI2V (ours)	-	1.509	0.443	1.726	77.265	65.806

Table 2: **Ablation study on model variants.**

Method	Plücker	Epipolar	3D Full	TransErr↓	RotErr↓	CamMC↓	FVD↓	
							VideoGPT	StyleGAN
	✓	✓		1.509	0.443	1.726	77.265	65.806
	✓		✓	1.605	0.497	1.851	70.068	60.830
DynamiCrafter+CamI2V (ours)	✓			1.516	0.482	1.757	72.069	61.999
		✓		4.613	1.844	5.799	107.97	91.318
			✓	6.627	3.677	9.287	115.36	100.58
DynamiCrafter				10.10	3.268	11.79	127.41	107.12

generated frames, witnessed by a large drop of FVD. We conclude that Plücker embedding serves as a more expressive position encoding and is more effective for the model to leverage geometric correspondence, thus better cross-frame consistency.

3D full attention alone without Plücker embedding. The use of 3D Full Attention alone, without employing Plücker embeddings to provide global positional encoding (a form of clean condition), fails to achieve camera controllability. This indicates that even with a 3D global receptive field, the presence of noise limits the model’s ability to generate videos that follow specific camera trajectories, resulting instead in random video generation that conforms to the dataset distribution.

Epipolar attention alone without Plücker embedding. The use of Epipolar Attention alone, without Plücker embeddings for global positional encoding (a form of clean condition), still retains a degree of camera controllability. This notable phenomenon suggests that explicit constraints can enable the model to grasp knowledge about the physical world.

3D full attention along with Plücker embedding. The use of 3D full attention with employing Plücker embeddings to provide global positional encoding (a form of clean condition), achieves the best FVD but results in the poorest camera controllability metrics. This supports our earlier discussion in the introduction that 3D full attention loses its ability to track features under high noise conditions. However, in small noise scenarios, it can access a greater number of features, allowing for the generation of videos that conform to the dataset distribution, though these may not align with the camera trajectories provided by users.

Epipolar attention along with Plücker embedding. When the explicit constraint of Epipolar Attention is combined with the implicit prior provided by Plücker embeddings for global positional encoding, the best camera controllability is achieved. This underscores the necessity of explicit constraints like Epipolar Attention. Although the FVD declines, this is understandable; when FVD reaches a saturation point, enhancing controllability inevitably leads to deviations from the current distribution. Achieving the best FVD with 3D Full Attention alone, without controllability, lacks practical value in the field of controllable generation.

5.4 QUALITATIVE COMPARISON

Visualization on RealEstate10K. As shown in Fig. 7, we present the visualization results of DynamiCrafter, MotionCtrl, CameraCtrl and our CamI2V. It can be observed that the camera trajectory of our method aligns more closely with GT compared with other methods, and the rendering of certain details appears more realistic in the video generated by our CamI2V.

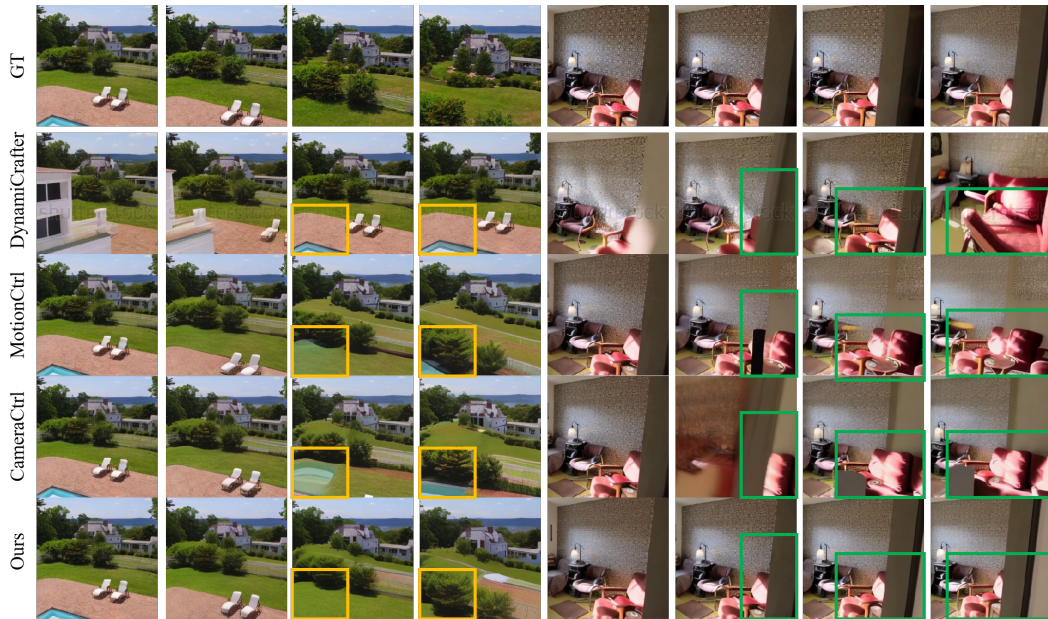


Figure 7: Qualitative Comparison on RealEstate10K.



Figure 8: Out-of-Domain Visualization.

Out-of-domain visualization. Our CamI2V demonstrates strong generalization capabilities, enabling direct application to camera controlled video generation across out-of-domain content, such as oil paintings, photography, and animation, as shown in Fig. 8.

6 CONCLUSION

In this paper, we address the integration of camera poses into diffusion models to enhance their understanding of the physical world in text-guided image-to-video generation. We propose a novel framework utilizing Plücker coordinates as 3D ray embeddings and introduce an epipolar attention mechanism that aggregates features along epipolar lines, ensuring robust tracking even under high noise conditions. Additionally, we incorporate register tokens to manage scenarios where frames lack intersections due to rapid camera movements or occlusions. Our methods significantly improve controllability and stability, achieving state-of-the-art performance on RealEstate10K and out-of-domain datasets. However, challenges remain in high-resolution generation, handling complex camera trajectories, and maintaining generation quality in long videos. Future work will focus on these aspects, alongside releasing checkpoints and training/evaluation codes to support further research.

REFERENCES

- Andreas Blattmann, Tim Dockhorn, Sumith Kulal, Daniel Mendelevitch, Maciej Kilian, Dominik Lorenz, Yam Levi, Zion English, Vikram Voleti, Adam Letts, et al. Stable video diffusion: Scaling latent video diffusion models to large datasets. *arXiv preprint arXiv:2311.15127*, 2023a.
- Andreas Blattmann, Robin Rombach, Huan Ling, Tim Dockhorn, Seung Wook Kim, Sanja Fidler, and Karsten Kreis. Align your latents: High-resolution video synthesis with latent diffusion models. In *Proceedings of the IEEE/CVF Conference on Computer Vision and Pattern Recognition*, pp. 22563–22575, 2023b.
- Tim Brooks, Bill Peebles, Connor Holmes, Will DePue, Yufei Guo, Li Jing, David Schnurr, Joe Taylor, Troy Luhman, Eric Luhman, Clarence Ng, Ricky Wang, and Aditya Ramesh. Video generation models as world simulators. 2024. URL <https://openai.com/research/video-generation-models-as-world-simulators>.
- Hila Chefer, Shiran Zada, Roni Paiss, Ariel Ephrat, Omer Tov, Michael Rubinstein, Lior Wolf, Tali Dekel, Tomer Michaeli, and Inbar Mosseri. Still-moving: Customized video generation without customized video data. *arXiv preprint arXiv:2407.08674*, 2024.
- Changu Chen, Junwei Shu, Lianggangxu Chen, Gaoqi He, Changbo Wang, and Yang Li. Motion-zero: Zero-shot moving object control framework for diffusion-based video generation. *arXiv preprint arXiv:2401.10150*, 2024a.
- Haoxin Chen, Menghan Xia, Yingqing He, Yong Zhang, Xiaodong Cun, Shaoshu Yang, Jinbo Xing, Yaofang Liu, Qifeng Chen, Xintao Wang, et al. Videocrafter1: Open diffusion models for high-quality video generation. *arXiv preprint arXiv:2310.19512*, 2023a.
- Haoxin Chen, Yong Zhang, Xiaodong Cun, Menghan Xia, Xintao Wang, Chao Weng, and Ying Shan. Videocrafter2: Overcoming data limitations for high-quality video diffusion models. In *Proceedings of the IEEE/CVF Conference on Computer Vision and Pattern Recognition*, pp. 7310–7320, 2024b.
- Xinyuan Chen, Yaohui Wang, Lingjun Zhang, Shaobin Zhuang, Xin Ma, Jiashuo Yu, Yali Wang, Dahua Lin, Yu Qiao, and Ziwei Liu. Seine: Short-to-long video diffusion model for generative transition and prediction. In *The Twelfth International Conference on Learning Representations*, 2023b.
- Prafulla Dhariwal and Alexander Nichol. Diffusion models beat gans on image synthesis. *Advances in neural information processing systems*, 34:8780–8794, 2021.
- Patrick Esser, Johnathan Chiu, Parmida Atighehchian, Jonathan Granskog, and Anastasis Germanidis. Structure and content-guided video synthesis with diffusion models. In *Proceedings of the IEEE/CVF International Conference on Computer Vision*, pp. 7346–7356, 2023.
- Songwei Ge, Seungjun Nah, Guilin Liu, Tyler Poon, Andrew Tao, Bryan Catanzaro, David Jacobs, Jia-Bin Huang, Ming-Yu Liu, and Yogesh Balaji. Preserve your own correlation: A noise prior for video diffusion models. In *Proceedings of the IEEE/CVF International Conference on Computer Vision*, pp. 22930–22941, 2023.
- Rohit Girdhar, Mannat Singh, Andrew Brown, Quentin Duval, Samaneh Azadi, Sai Saketh Rambhatla, Akbar Shah, Xi Yin, Devi Parikh, and Ishan Misra. Emu video: Factorizing text-to-video generation by explicit image conditioning. *arXiv preprint arXiv:2311.10709*, 2023.
- Yuwei Guo, Ceyuan Yang, Anyi Rao, Zhengyang Liang, Yaohui Wang, Yu Qiao, Maneesh Agrawala, Dahua Lin, and Bo Dai. Animatediff: Animate your personalized text-to-image diffusion models without specific tuning. *arXiv preprint arXiv:2307.04725*, 2023.
- Hao He, Yinghao Xu, Yuwei Guo, Gordon Wetzstein, Bo Dai, Hongsheng Li, and Ceyuan Yang. Cameractrl: Enabling camera control for text-to-video generation. *arXiv preprint arXiv:2404.02101*, 2024a.

- Xu He, Qiaochu Huang, Zhensong Zhang, Zhiwei Lin, Zhiyong Wu, Sicheng Yang, Minglei Li, Zhiyi Chen, Songcen Xu, and Xiaofei Wu. Co-speech gesture video generation via motion-decoupled diffusion model. In *Proceedings of the IEEE/CVF Conference on Computer Vision and Pattern Recognition*, pp. 2263–2273, 2024b.
- Yingqing He, Tianyu Yang, Yong Zhang, Ying Shan, and Qifeng Chen. Latent video diffusion models for high-fidelity long video generation. *arXiv preprint arXiv:2211.13221*, 2022.
- Jonathan Ho and Tim Salimans. Classifier-free diffusion guidance. *arXiv preprint arXiv:2207.12598*, 2022.
- Jonathan Ho, Ajay Jain, and Pieter Abbeel. Denoising diffusion probabilistic models. *Advances in neural information processing systems*, 33:6840–6851, 2020.
- Edward J Hu, Yelong Shen, Phillip Wallis, Zeyuan Allen-Zhu, Yuezhi Li, Shean Wang, Lu Wang, and Weizhu Chen. Lora: Low-rank adaptation of large language models. *arXiv preprint arXiv:2106.09685*, 2021.
- Li Hu. Animate anyone: Consistent and controllable image-to-video synthesis for character animation. In *Proceedings of the IEEE/CVF Conference on Computer Vision and Pattern Recognition*, pp. 8153–8163, 2024.
- Teng Hu, Jiangning Zhang, Ran Yi, Yating Wang, Hongrui Huang, Jieyu Weng, Yabiao Wang, and Lizhuang Ma. Motionmaster: Training-free camera motion transfer for video generation. *arXiv preprint arXiv:2404.15789*, 2024.
- Yash Jain, Anshul Nasery, Vibhav Vineet, and Harkirat Behl. Peekaboo: Interactive video generation via masked-diffusion. In *Proceedings of the IEEE/CVF Conference on Computer Vision and Pattern Recognition*, pp. 8079–8088, 2024.
- Rui Jiang, Guang-Cong Zheng, Teng Li, Tian-Rui Yang, Jing-Dong Wang, and Xi Li. A survey of multimodal controllable diffusion models. *Journal of Computer Science and Technology*, 39(3): 509–541, 2024.
- Zhengqi Li, Richard Tucker, Noah Snively, and Aleksander Holynski. Generative image dynamics. In *Proceedings of the IEEE/CVF Conference on Computer Vision and Pattern Recognition*, pp. 24142–24153, 2024.
- Ruoshi Liu, Rundi Wu, Basile Van Hoorick, Pavel Tokmakov, Sergey Zakharov, and Carl Vondrick. Zero-1-to-3: Zero-shot one image to 3d object. In *Proceedings of the IEEE/CVF international conference on computer vision*, pp. 9298–9309, 2023.
- Xin Ma, Yaohui Wang, Gengyun Jia, Xinyuan Chen, Ziwei Liu, Yuan-Fang Li, Cunjian Chen, and Yu Qiao. Latte: Latent diffusion transformer for video generation. *arXiv preprint arXiv:2401.03048*, 2024a.
- Yue Ma, Yingqing He, Xiaodong Cun, Xintao Wang, Siran Chen, Xiu Li, and Qifeng Chen. Follow your pose: Pose-guided text-to-video generation using pose-free videos. In *Proceedings of the AAAI Conference on Artificial Intelligence*, volume 38, pp. 4117–4125, 2024b.
- Chenlin Meng, Robin Rombach, Ruiqi Gao, Diederik Kingma, Stefano Ermon, Jonathan Ho, and Tim Salimans. On distillation of guided diffusion models. In *Proceedings of the IEEE/CVF Conference on Computer Vision and Pattern Recognition*, pp. 14297–14306, 2023.
- Chong Mou, Xintao Wang, Liangbin Xie, Yanze Wu, Jian Zhang, Zhongang Qi, and Ying Shan. T2i-adapter: Learning adapters to dig out more controllable ability for text-to-image diffusion models. In *Proceedings of the AAAI Conference on Artificial Intelligence*, volume 38, pp. 4296–4304, 2024.
- Linfei Pan, Daniel Barath, Marc Pollefeys, and Johannes Lutz Schönberger. Global Structure-from-Motion Revisited. In *European Conference on Computer Vision (ECCV)*, 2024.
- William Peebles and Saining Xie. Scalable diffusion models with transformers. In *Proceedings of the IEEE/CVF International Conference on Computer Vision*, pp. 4195–4205, 2023.

- Bohao Peng, Jian Wang, Yuechen Zhang, Wenbo Li, Ming-Chang Yang, and Jiaya Jia. Controlnext: Powerful and efficient control for image and video generation. *arXiv preprint arXiv:2408.06070*, 2024.
- Julius Plücker. *Analytisch-Geometrische Entwicklungen*, volume 2. GD Baedeker, 1828.
- Aditya Ramesh, Prafulla Dhariwal, Alex Nichol, Casey Chu, and Mark Chen. Hierarchical text-conditional image generation with clip latents. *arXiv preprint arXiv:2204.06125*, 2022.
- Robin Rombach, Andreas Blattmann, Dominik Lorenz, Patrick Esser, and Björn Ommer. High-resolution image synthesis with latent diffusion models. 2022.
- Johannes L Schonberger and Jan-Michael Frahm. Structure-from-motion revisited. In *Proceedings of the IEEE conference on computer vision and pattern recognition*, pp. 4104–4113, 2016.
- Kunpeng Song, Yizhe Zhu, Bingchen Liu, Qing Yan, Ahmed Elgammal, and Xiao Yang. Moma: Multimodal llm adapter for fast personalized image generation. *arXiv preprint arXiv:2404.05674*, 2024.
- Yang Song, Jascha Sohl-Dickstein, Diederik P Kingma, Abhishek Kumar, Stefano Ermon, and Ben Poole. Score-based generative modeling through stochastic differential equations. *arXiv preprint arXiv:2011.13456*, 2020.
- Boshi Tang, Jianan Wang, Zhiyong Wu, and Lei Zhang. Stable score distillation for high-quality 3d generation. *arXiv preprint arXiv:2312.09305*, 2023a.
- Zineng Tang, Ziyi Yang, Chenguang Zhu, Michael Zeng, and Mohit Bansal. Any-to-any generation via composable diffusion. In *Thirty-seventh Conference on Neural Information Processing Systems*, 2023b. URL <https://openreview.net/forum?id=2EDqbSCnmF>.
- Linrui Tian, Qi Wang, Bang Zhang, and Liefeng Bo. Emo: Emote portrait alive-generating expressive portrait videos with audio2video diffusion model under weak conditions. *arXiv preprint arXiv:2402.17485*, 2024.
- Darcet Timothée, Oquab Maxime, Mairal Julien, and Bojanowski Piotr. Vision transformers need registers. In *The Twelfth International Conference on Learning Representations*, 2024.
- Hung-Yu Tseng, Qinbo Li, Changil Kim, Suhub Alsisan, Jia-Bin Huang, and Johannes Kopf. Consistent view synthesis with pose-guided diffusion models. In *Proceedings of the IEEE/CVF Conference on Computer Vision and Pattern Recognition*, pp. 16773–16783, 2023.
- Thomas Unterthiner, Sjoerd Van Steenkiste, Karol Kurach, Raphael Marinier, Marcin Michalski, and Sylvain Gelly. Towards accurate generative models of video: A new metric & challenges. *arXiv preprint arXiv:1812.01717*, 2018.
- Jiuniu Wang, Hangjie Yuan, Dayou Chen, Yingya Zhang, Xiang Wang, and Shiwei Zhang. Mod-elscope text-to-video technical report. *arXiv preprint arXiv:2308.06571*, 2023a.
- Tan Wang, Linjie Li, Kevin Lin, Chung-Ching Lin, Zhengyuan Yang, Hanwang Zhang, Zicheng Liu, and Lijuan Wang. Disco: Disentangled control for referring human dance generation in real world. *arXiv e-prints*, pp. arXiv–2307, 2023b.
- Wenjing Wang, Huan Yang, Zixi Tuo, Huiguo He, Junchen Zhu, Jianlong Fu, and Jiaying Liu. Videofactory: Swap attention in spatiotemporal diffusions for text-to-video generation, 2024a. URL <https://openreview.net/forum?id=dUDwK38MVC>.
- Xiang Wang, Hangjie Yuan, Shiwei Zhang, Dayou Chen, Jiuniu Wang, Yingya Zhang, Yujun Shen, Deli Zhao, and Jingren Zhou. Videocomposer: Compositional video synthesis with motion controllability. *Advances in Neural Information Processing Systems*, 36, 2024b.
- Yaohui Wang, Xinyuan Chen, Xin Ma, Shangchen Zhou, Ziqi Huang, Yi Wang, Ceyuan Yang, Yinan He, Jiashuo Yu, Peiqing Yang, et al. Lavie: High-quality video generation with cascaded latent diffusion models. *arXiv preprint arXiv:2309.15103*, 2023c.

- Zhao Wang, Aoxue Li, Enze Xie, Lingting Zhu, Yong Guo, Qi Dou, and Zhenguo Li. Customvideo: Customizing text-to-video generation with multiple subjects. *arXiv preprint arXiv:2401.09962*, 2024c.
- Zhouxia Wang, Ziyang Yuan, Xintao Wang, Yaowei Li, Tianshui Chen, Menghan Xia, Ping Luo, and Ying Shan. Motionctrl: A unified and flexible motion controller for video generation. In *ACM SIGGRAPH 2024 Conference Papers*, pp. 1–11, 2024d.
- Jianzong Wu, Xiangtai Li, Yanhong Zeng, Jiangning Zhang, Qianyu Zhou, Yining Li, Yunhai Tong, and Kai Chen. Motionbooth: Motion-aware customized text-to-video generation. *arXiv preprint arXiv:2406.17758*, 2024a.
- Tao Wu, Xuewei Li, Zhongang Qi, Di Hu, Xintao Wang, Ying Shan, and Xi Li. Spherediffusion: Spherical geometry-aware distortion resilient diffusion model. In *Proceedings of the AAAI Conference on Artificial Intelligence*, volume 38, pp. 6126–6134, 2024b.
- Tao Wu, Yong Zhang, Xintao Wang, Xianpan Zhou, Guangcong Zheng, Zhongang Qi, Ying Shan, and Xi Li. Customcrafter: Customized video generation with preserving motion and concept composition abilities. *arXiv preprint arXiv:2408.13239*, 2024c.
- Yinwei Wu, Xianpan Zhou, Bing Ma, Xuefeng Su, Kai Ma, and Xinchao Wang. Ifadapter: Instance feature control for grounded text-to-image generation. *arXiv preprint arXiv:2409.08240*, 2024d.
- Jinbo Xing, Menghan Xia, Yong Zhang, Haoxin Chen, Xintao Wang, Tien-Tsin Wong, and Ying Shan. Dynamicrafter: Animating open-domain images with video diffusion priors. *arXiv preprint arXiv:2310.12190*, 2023.
- Dejia Xu, Weili Nie, Chao Liu, Sifei Liu, Jan Kautz, Zhangyang Wang, and Arash Vahdat. Camco: Camera-controllable 3d-consistent image-to-video generation. *arXiv preprint arXiv:2406.02509*, 2024a.
- Zhongcong Xu, Jianfeng Zhang, Jun Hao Liew, Hanshu Yan, Jia-Wei Liu, Chenxu Zhang, Jiashi Feng, and Mike Zheng Shou. Magicanimate: Temporally consistent human image animation using diffusion model. In *Proceedings of the IEEE/CVF Conference on Computer Vision and Pattern Recognition*, pp. 1481–1490, 2024b.
- Shiyuan Yang, Liang Hou, Haibin Huang, Chongyang Ma, Pengfei Wan, Di Zhang, Xiaodong Chen, and Jing Liao. Direct-a-video: Customized video generation with user-directed camera movement and object motion. In *ACM SIGGRAPH 2024 Conference Papers*, pp. 1–12, 2024a.
- Zhuoyi Yang, Jiayan Teng, Wendi Zheng, Ming Ding, Shiyu Huang, Jiazheng Xu, Yuanming Yang, Wenyi Hong, Xiaohan Zhang, Guanyu Feng, et al. Cogvideox: Text-to-video diffusion models with an expert transformer. *arXiv preprint arXiv:2408.06072*, 2024b.
- Hu Ye, Jun Zhang, Sibao Liu, Xiao Han, and Wei Yang. Ip-adapter: Text compatible image prompt adapter for text-to-image diffusion models. *arXiv preprint arXiv:2308.06721*, 2023.
- Shengming Yin, Chenfei Wu, Jian Liang, Jie Shi, Houqiang Li, Gong Ming, and Nan Duan. Drag-nuwa: Fine-grained control in video generation by integrating text, image, and trajectory. *arXiv preprint arXiv:2308.08089*, 2023.
- Sihyun Yu, Weili Nie, De-An Huang, Boyi Li, Jinwoo Shin, and Anima Anandkumar. Efficient video diffusion models via content-frame motion-latent decomposition. *arXiv preprint arXiv:2403.14148*, 2024.
- Lvmin Zhang, Anyi Rao, and Maneesh Agrawala. Adding conditional control to text-to-image diffusion models. In *Proceedings of the IEEE/CVF International Conference on Computer Vision*, pp. 3836–3847, 2023a.
- Shiwei Zhang, Jiayu Wang, Yingya Zhang, Kang Zhao, Hangjie Yuan, Zhiwu Qin, Xiang Wang, Deli Zhao, and Jingren Zhou. I2vgen-xl: High-quality image-to-video synthesis via cascaded diffusion models. *arXiv preprint arXiv:2311.04145*, 2023b.

- Yiming Zhang, Zhening Xing, Yanhong Zeng, Youqing Fang, and Kai Chen. Pia: Your personalized image animator via plug-and-play modules in text-to-image models. In *Proceedings of the IEEE/CVF Conference on Computer Vision and Pattern Recognition*, pp. 7747–7756, 2024.
- Guangcong Zheng, Shengming Li, Hui Wang, Taiping Yao, Yang Chen, Shouhong Ding, and Xi Li. Entropy-driven sampling and training scheme for conditional diffusion generation. In *European Conference on Computer Vision*, pp. 754–769. Springer, 2022.
- Guangcong Zheng, Xianpan Zhou, Xuwei Li, Zhongang Qi, Ying Shan, and Xi Li. Layoutdiffusion: Controllable diffusion model for layout-to-image generation. In *Proceedings of the IEEE/CVF Conference on Computer Vision and Pattern Recognition*, pp. 22490–22499, 2023.
- Zangwei Zheng, Xiangyu Peng, and Yang You. Open-sora: Democratizing efficient video production for all, March 2024. URL <https://github.com/hpcaitech/Open-Sora>.
- Tinghui Zhou, Richard Tucker, John Flynn, Graham Fyffe, and Noah Snavely. Stereo magnification: Learning view synthesis using multiplane images. In *SIGGRAPH*, 2018.

A CORE CODES

Algorithm 1 Spatial Attention Block

Require: U-Net feature x , condition c

- 1: $x \leftarrow x + \text{SelfAttn}_1(\text{PreNorm}(x))$
- 2: $x \leftarrow x + \text{CrossAttn}_2(\text{PreNorm}(x), c)$
- 3: $x \leftarrow x + \text{FFN}(\text{PreNorm}(x))$
- 4: **return** x

Algorithm 2 Temporal Attention Block with Camera Control

Require: U-Net feature x , condition c , Plücker embedding p , epipolar attention mask m

- 1: $x \leftarrow x + \text{Linear}(\text{PreNorm}(x) + \text{PreNorm}(p))$ ▷ Pücker Ray Embeddings
- 2: $x \leftarrow x + \text{EpipolarAttn}(\text{PreNorm}(x), m)$
- 3: $x \leftarrow x + \text{SelfAttn}_1(\text{PreNorm}(x))$
- 4: $x \leftarrow x + \text{SelfAttn}_2(\text{PreNorm}(x))$
- 5: $x \leftarrow x + \text{FFN}(\text{PreNorm}(x))$
- 6: **return** x

Algorithm 3 Epipolar Attention Mask

Require: Intrinsic matrices K , extrinsic matrices $[R|T]$, feature size $H \times W$, threshold δ

- 1: $E \leftarrow T \times R$ ▷ Essential matrices E
- 2: $F \leftarrow K^{-T} \cdot E \cdot K^{-1}$ ▷ Fundamental matrices F
- 3: $g \leftarrow \text{mesh_grid}(H, W)$ ▷ Homogeneous feature coordinates g
- 4: $l \leftarrow \text{normalize}(F \cdot g^T)$ ▷ Epipolar line $l = Ax + By + C$, normalized by $\sqrt{A^2 + B^2}$
- 5: $d \leftarrow l^T \cdot g^T$ ▷ Distance d from feature coordinates to epipolar lines
- 6: $m \leftarrow [\text{reg}] \oplus \text{flatten}(d < \delta)$ ▷ Epipolar attention mask m
- 7: **return** m

B COLMAP & GLOMAP CONFIGURATION

We assume `SIMPLE_PINHOLE` as the common camera model for all video clips and all 16 frames from the same video clip share the same camera intrinsics. For the feature extractor, we enable `estimate_affine_shape` and `domain_size_pooling` in `SiftExtraction`, while fix camera intrinsics by passing (f_x, f_y, c_x, c_y) into `ImageReader.camera_params`. For the exhaustive matcher, we enable `guided_matching` and set `max_num_matches` to 65536 in `SiftMatching` to make possible more underlying matches. For the global mapper, we disable `BundleAdjustment.optimize_intrinsics` and relax the geometric constraint by extending `RelPoseEstimation.max_epipolar_error` to 4.

C GPU MEMORY AND SPEED

Table 3: **Comparison on GPU memory usage and speed under DeepSpeed ZeRO-1.** * denotes our reproduction on DynamiCrafter. We report full parameter fine-tuning results of DynamiCrafter. Our model can be trained on 24GB custom-level GPUs despite the additional epipolar attention.

Method	# Trainable Parameters	GPU Memory (GiB) ↓		Time (s) ↓		
		Inference	Training	Forward	Backward	Optimizer
DynamiCrafter	1.4 B	11.14	23.72	0.413	0.856	1.959
DynamiCrafter+MotionCtrl*	63.4 M	11.18	16.75	0.387	0.198	0.636
DynamiCrafter+CameraCtrl*	211 M	11.56	18.44	0.398	0.247	0.723
DynamiCrafter+CamI2V (ours)	261 M	11.67	21.71	0.403	0.458	0.974

D EXTRA OUT-OF-DOMAIN VISUALIZATIONS



Figure 9: Orbit right on unseen images.



Figure 10: Zoom in on unseen images.

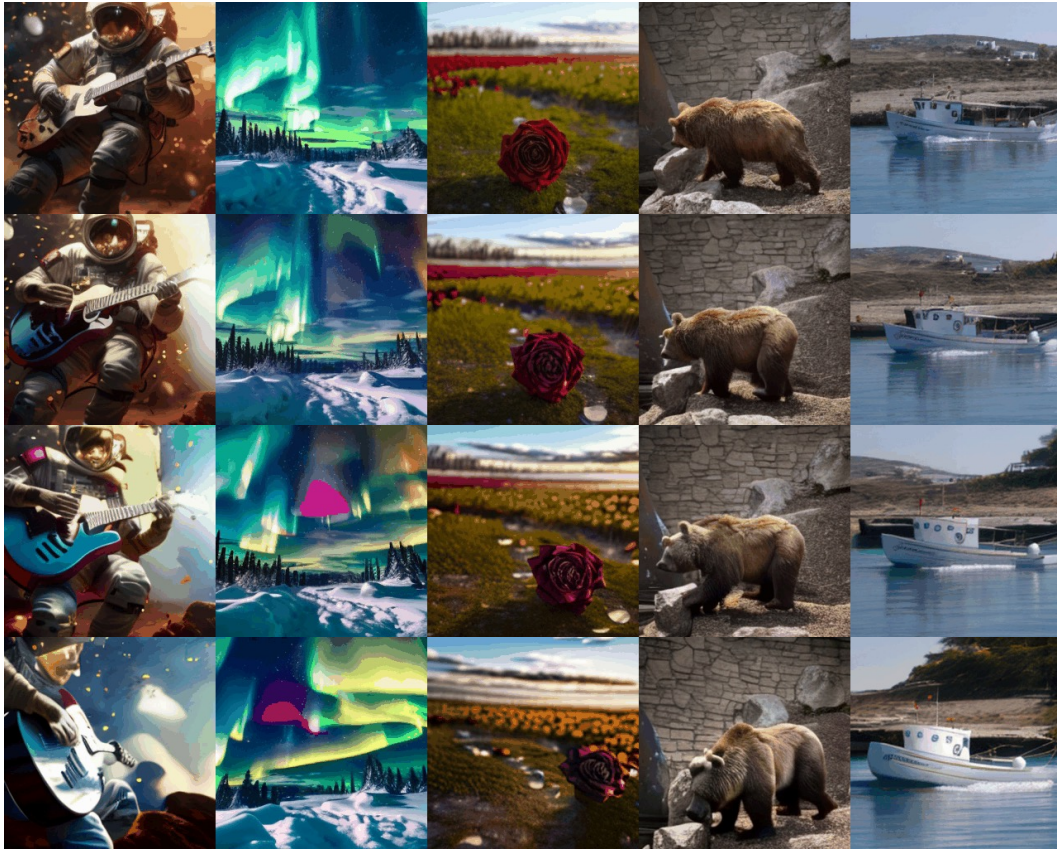


Figure 11: Orbit left on unseen images.

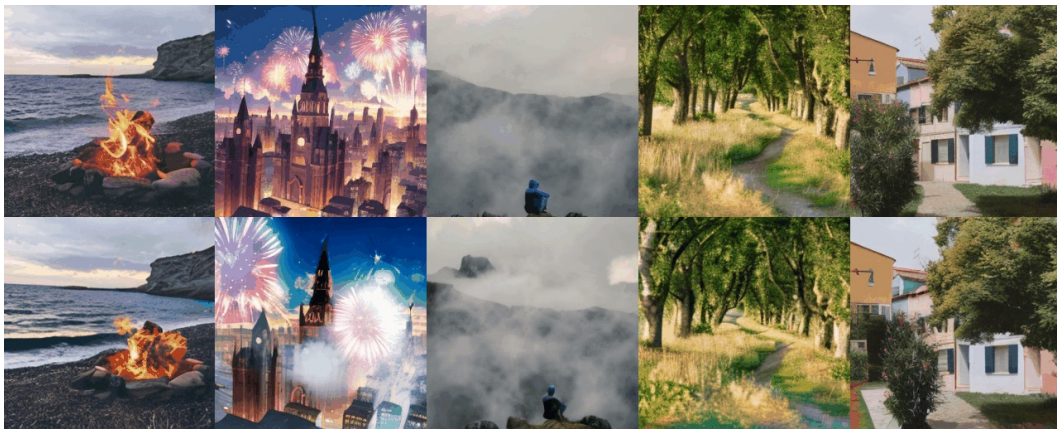


Figure 12: Zoom out on unseen images.

E EXTRA REALESTATE10K VISUALIZATIONS



Figure 13: Extra RealEstate10K Visualizations.